The Astronomical Journal, 140:913–918, 2010 October doi:10.1088/0004-6256/140/4/913

AN EXPANDING H I PHOTODISSOCIATED REGION ASSOCIATED WITH THE COMPACT H II REGION G213.880−11.837 IN THE GGD 14 COMPLEX

Y. Gómez[1], G. Garay[2], C. A. Rodríguez-Rico[3], C. Neria[1], L. F. Rodríguez[1], V. Escalante[1], S. Lizano[1], and M. Lebrón[4]
[1] Centro de Radioastronomía y Astrofísica, UNAM, Apartado Postal 3-72, Morelia, Michoacán 58089, Mexico;
y.gomez@crya.unam.mx, c.neria@crya.unam.mx, l.rodriguez@crya.unam.mx, v.escalante@crya.unam.mx, s.lizano@crya.unam.mx
[2] Departamento de Astronomía, Universidad de Chile, Casilla 36-D, Santiago, Chile; guido@das.uchile.cl
[3] Departamento de Astronomía, Universidad de Guanajuato, Apartado Postal 144, Guanajuato, GTO 36240, Mexico; carlos@astro.ugto.mx
[4] Departamento de Ciencias Físicas, Universidad de Puerto Rico, P.O. Box 23323, San Juan, PR 00931-3323, USA; mayra.lebron3@upr.edu
Received 2010 June 4; accepted 2010 July 12; published 2010 August 17

ABSTRACT

We present high angular and spectral resolution H I 21 cm line observations toward the cometary-shaped compact H II region G213.880−11.837 in the GGD 14 complex. The kinematics and morphology of the photodissociated region, traced by the H I line emission, reveal that the neutral gas is part of an expanding flow. The kinematics of the H I gas along the major axis of G213.880−11.837 shows that the emission is very extended toward the SE direction, reaching local standard of rest (LSR) radial velocities in the tail of about 14 km s^{-1}. The ambient LSR radial velocity of the molecular gas is 11.5 km s^{-1}, which suggests a champagne flow of the H I gas. This is the second (after G111.61+0.37) cometary H II/H I region known.

Key words: H II regions – ISM: individual objects (GGD 12-15, GGD 14, G213.880−11.837) – radio lines: ISM

1. INTRODUCTION

The spatial morphology, abundance, and kinematics of the neutral gas around compact H II (CH II) regions and its relation with other physical parameters remain poorly studied for most H II regions. To date, only a few photodissociated regions (PDRs) have been observed at radio wavelengths with high angular resolution (e.g., Lebrón & Rodríguez 1997; Gómez et al. 1998; Garay et al. 1998; Brogan et al. 1999; Lebrón et al. 2001; Cappa et al. 2008). GGD 14 is an active star-forming region, part of the group of red nebulous objects GGD 12/13/14/15 (Gyulbudaghian et al. 1978) embedded in the Monoceros molecular cloud at a distance of $d \sim 1$ kpc (Rodríguez et al. 1980). There is an extended (∼1.8 pc) bipolar outflow in the region, traced by CO emission with a major axis along the NW–SE direction (Rodríguez et al. 1982; Little et al. 1990; Qin et al. 2008). This bipolar outflow seems to be excited by a small region of free–free emission (named VLA 7 by Gómez et al. 2000), possibly a thermal jet (Eisloffel et al. 2000). The powering source of this bipolar outflow is also associated with an H_2O maser (Rodríguez et al. 1982), a hydrogen molecular emission object (Fang & Yao 2004) and coincident in position with a class I/0 source, recently detected in the mid-infrared (IRS 9Mc; Sato et al. 2008).

The GGD 14 star-forming region contains a cluster of radio sources dominated by the compact (∼0.01 pc) cometary-shaped H II region (VLA 1; G213.880−11.837), which is excited by a B0.5 ZAMS star (Rodríguez et al. 1980; Kurtz et al. 1994; Gómez et al. 1998, 2000, 2002) and is associated with IRAS 06084−0611. A detailed kinematic study of the gas within the cometary H II region, presented by Gómez et al. (1998), shows that the ionized gas is undergoing a champagne flow with the head of the ionized champagne flow located to the NW and the extended emission toward the SE. There is a velocity gradient along the major axis of the ionized champagne flow with the LSR radial velocity increasing from ∼11 km s^{-1} at the head of the flow to ∼15 km s^{-1} at the tail. In a champagne flow the velocity at the head is expected to be very similar to the velocity of the ambient molecular gas, and this is the case for the champagne flow in GGD 14 where the ambient velocity is about 11 km s^{-1} (Torrelles et al. 1989; Qin et al. 2008).

In addition of the ionized champagne flow, Gómez et al. (1998) reported the existence of an unresolved PDR surrounding the ionized gas. The distribution of the molecular gas in the GGD 14 region is complex with the presence of different velocity components (Rodríguez et al. 1980; Güsten & Marcaide 1986; Torrelles et al. 1989; Little et al. 1990; Anglada et al. 1996). Recent ^{13}CO(2→1) observations by Qin et al. (2008) toward the GGD 14 region show that the molecular emission peaks at a velocity of ∼11.5 km s^{-1} that could be considered as the velocity of the ambient molecular gas.

In the present work, we analyze new H I 21 cm line observations toward the cometary H II region G213.880−11.837 in GGD 14 with higher angular (15″) and spectral (∼1 km s^{-1}) resolution than the data presented by Gómez et al. (1998). These new observations resolve the morphology of the H I region that surrounds the ionized material. In Section 2 we present the observations, in Section 3 the results, in Section 4 an interpretation of the H I observations, and in Section 5 the conclusions.

2. OBSERVATIONS

The H I 21 cm ($\nu = 1420.406$ MHz) observations toward the star-forming region GGD 14 were made using the Very Large Array (VLA) of the NRAO.[5] The observations were taken on 1998 December 23 in the C configuration (under project AL459). The total bandwidth of 0.781 MHz was centered at a V_{LSR} of 12 km s^{-1}, with 256 channels 0.64 km s^{-1} wide each (3.1 kHz). Hanning smoothing was applied to the line resulting in a spectral resolution of ∼1.2 km s^{-1}. The flux density scale was determined from observations of the amplitude calibrator 0134+329, for which a flux density of 15.87 Jy was adopted. The phase calibrator was 0605−085 for which a bootstrapped 1.4 GHz flux density of 2.11 ± 0.01 Jy was obtained. The data were edited and calibrated following standard procedures and

[5] The National Radio Astronomy Observatory is operated by Associated Universities, Inc., under cooperative agreement with the National Science Foundation.

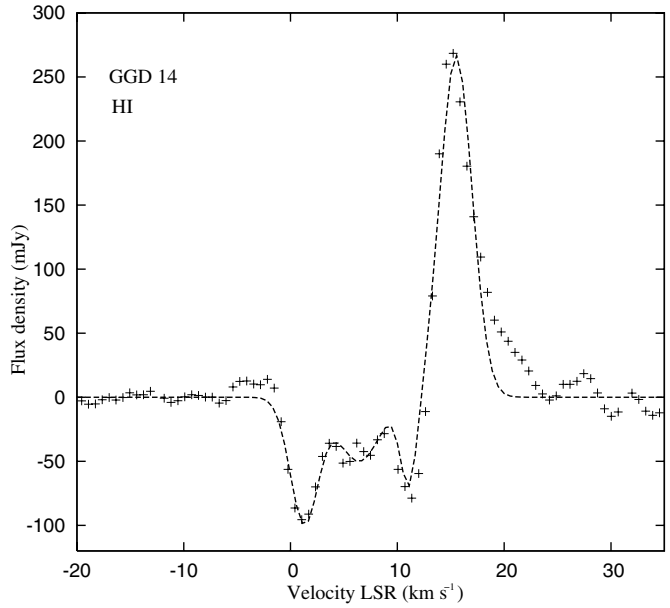

Figure 1. Integrated spectrum of the H I 21 cm line emission toward GGD 14. The dashed line shows the fit to the data with four Gaussians (see Table 1).

images were made using the NRAO software AIPS. Line images were made by subtracting the continuum (line-free) channels from the visibility data using the task UVLSF. The images were made with the task IMAGR, using the ROBUST parameter equal to zero (Briggs 1995), resulting in a synthesized beam of $17'' \times 14''$, P.A. $= -26°$. The rms noise level in a single spectral line channel, after Hanning smoothing, is $\sim$2.0 mJy beam^{-1}.

3. RESULTS

The detected radio continuum emission at 21 cm, made with the line-free channels, is marginally resolved ($4\farcs3 \times 2\farcs9$, P.A. $= 148°$) with a flux density of 72 ± 2 mJy and peak position at $\alpha(2000) = 06^{\rm h}10^{\rm m}50\fs607 \pm 0\fs004$, $\delta(2000) = -06°11'50\farcs10 \pm 0\farcs05$. The H I 21 cm line is detected both in absorption and emission in the velocity range from $\sim$1 to 20 km s^{-1} in agreement with previous results reported by Gómez et al. (1998).

Figure 1 shows the H I 21 cm spectrum integrated over the whole source in a box with size of $\sim 1\farcm3 \times 1\farcm3$. As was noted by Gómez et al. (1998), the H I absorption component is considerably broad toward blueshifted velocities, showing three minima and extending from velocities of -1 km s^{-1} to $\sim +12$ km s^{-1}. In Table 1, we present the results of a Gaussian fit for the three H I absorption components plus a single Gaussian for the emission component (the fit is shown as a dashed line in Figure 1). In this table we give the peak flux (S_l), the center velocity ($V_{\rm LSR}$), and the full width at half-maximum (FWHM) of the line (ΔV) for each Gaussian component. The H I absorption components are centered at $V_{\rm LSR}$ of $\sim$1, 6, and 11 km s^{-1} (see Table 1). On the other hand, the H I emission is present in a velocity range from $\sim$13 to 20 km s^{-1}, with the maximum centered at $V_{\rm LSR} = 15.5$ km s^{-1} (Figure 1 and Table 1).

Figure 2 shows individual channel images of the H I 21 cm line toward GGD 14. The unresolved H I absorption appears coincident with the 1.4 GHz continuum peak position (named VLA 1 by Gómez et al. 2000) marked with a cross. The triangle, toward the NE of the CH II region, indicates the radio continuum peak position of the radio source VLA 7, which has been proposed as the exciting source of the bipolar outflow (Gómez et al. 2000, 2002) and is coincident with the H_2O maser emission in the region (Rodríguez et al. 1980). As observed in the H I line in emission, the PDR in GGD 14 appears spatially resolved with a deconvolved angular size of $45'' \times 40''$, P.A. $= 34°$ ($\sim$0.2 pc), and with a peak intensity spatially shifted toward the SE side of the cometary H II region (the PDR peaks at $\alpha(2000) = 06^{\rm h}10^{\rm m}51\fs3$, $\delta(2000) = -06°11'52'' \pm 2''$, about 0.1 pc in projected separation from the peak of the CH II region).

Table 1
Gaussian Components in the Fit to the H I Line Profile

S_l (mJy)	$V_{\rm LSR}$ (km s^{-1})	ΔV (km s^{-1})
-98 ± 36	1.2 ± 0.6	3 ± 1
-49 ± 24	6.4 ± 1.5	5 ± 3
-69 ± 27	11.1 ± 0.6	2 ± 1
267 ± 18	15.5 ± 0.1	4 ± 1

4. DISCUSSION

4.1. Physical Parameters of the H I Line

The individual H I 21 cm channels, toward GGD 14 (Figure 2), show an extended emission component toward the SE and a strong line absorption coincident with the cometary H II region. The PDR, traced by the H I region, is thus being produced mainly by the B0.5 ZAMS star that also ionizes the cometary H II region (VLA 1; G213.880−11.837).

It is possible to estimate the H I optical depth toward the CH II region using the H I absorption profile. Assuming that the continuum source is located behind a homogeneous H I cloud, the observed line brightness temperature is given by (see Rohlfs & Wilson 2003)

$$T_L(v) = (f_{\rm H\,I} T_{\rm ex} - f_0 f_c T_c)(1 - e^{-\tau_L(v)}),$$

where $T_{\rm ex}$ is the excitation temperature of the H I, T_c is the continuum brightness temperature of the CH II region at the frequency of the H I line, $f_{\rm H\,I}$ and f_c are the beam filling factors of the H I and the continuum, f_0 is the fraction of the continuum source covered by the H I cloud, and $\tau_L(v)$ is the optical depth of the H I gas at a velocity v. In this case, we consider that the continuum source is completely covered by the H I cloud, $f_0 = 1$. The estimation of the filling factor commonly uses a comparison between the beam solid angle (Ω_B) with the source solid angle (Ω_c), such that $f_c \simeq \Omega_c/\Omega_B$, but other geometric factors can be included.

Since the H I cloud shows a velocity gradient across the region (see Figure 2), we will assume that at the velocity of the absorption feature ($V_{\rm LSR} \simeq 11$ km s^{-1}), we only have to take into account the effect of the absorbing gas, neglecting the contribution to the emission ($f_{\rm H\,I} T_{\rm ex} \sim 0$), since this occurs mostly at other velocities. Then, the transfer equation at the center of the absorbing line is

$$T_L(0) = (-f_c T_c)(1 - e^{-\tau_L(0)}).$$

The resulting optical depth value is obtained using the expression

$$\tau_L(0) = -\ln\left(1 - \frac{|T_L(0)|}{f_c T_c}\right).$$

The beam-averaged brightness temperature of the continuum can be computed from the total flux density ($S_c \simeq 72$ mJy) and

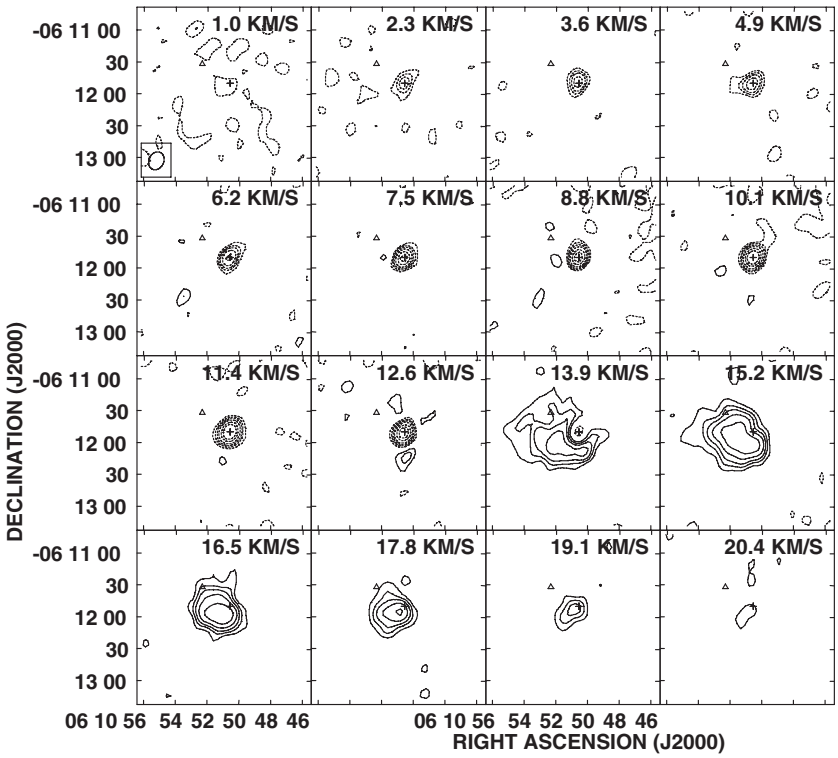

Figure 2. Individual channel images of the 21 cm H I emission and absorption toward the GGD 14 region. One out of every two channels was plotted. Contour levels are −20, −15, −10, −7, −3, 3, 5, 7, 10, and 15 × 2 mJy beam^{-1}, the rms noise of the images. The continuous and dashed contours indicate emission and absorption, respectively. The cross and the triangle mark the position of the radio continuum peak at 1.4 GHz of VLA 1 (G213.880−11.837) and VLA 7 (Gómez et al. 2000), respectively.

the deconvolved angular size measured in the 1.4 GHz continuum image ($\theta_c \simeq 3\farcs5$) by the expression $T_c = 688(S_\nu/\Omega_c)$, with $\Omega_c = 1.13\theta_c^2$, obtaining $T_c = 3600$ K. The filling factor is $f_c \simeq \theta_c^2/\theta_B^2$, where θ_B^2 is the beam size ($\sim 15\farcs4$), thus $f_c = 0.05$. The observed line brightness temperature, at the center of the absorbing line $T_L(0)$ for $S_L(0) = -69$ mJy and $\theta_B = 15\farcs4$, is −177 K. Then the mean optical depth has a very large value $\tau_L(0) \simeq 5$. As we note, the derived values for $T_L(0)$ and f_cT_c are similar, such that the ratio $T_L(0)/f_cT_c$ will be very close to unity, making the estimation of the optical depth very uncertain. Moreover, if we include the uncertainty in the estimated angular size and temperatures, the error in the mean optical depth will be around 60%, $\tau_L(0) \simeq 5 \pm 3$.

A lower limit to the H I mean density can be set by assuming an optical depth, $\tau_L(0) \gg 1$. This assumption is supported by our previous estimate, $\tau_L(0) \sim 5$, but with large uncertainties. Then taking simply $\tau_L(0) \geqslant 1$, $T_{\rm ex} \simeq 300$ K, and the FWHM of the line $\Delta V = 2$ km s^{-1} (see Table 1), we can estimate a lower limit for the H I column density, computed in the standard way (Rohlfs & Wilson 2003),

$$\left[\frac{N_{\rm H\,I}}{\rm cm^{-2}}\right] = 1.8224 \times 10^{18} \left[\frac{T_{\rm ex}}{\rm K}\right] \tau_L(0) \left[\frac{\Delta V}{\rm km\ s^{-1}}\right],$$

giving $N_{\rm H\,I} \geqslant 1.1 \times 10^{21}$ cm^{-2}. This column density is consistent with that expected for PDRs (Hollenbach & Tielens 1997). We will further assume that the physical depth of the region producing the H I absorption is approximately one-half of the diameter of the H I in emission ($\sim 42''$; $\simeq 0.2$ pc). Therefore, an estimate of the average neutral hydrogen density, $\langle n_{\rm H\,I}\rangle \simeq N_{\rm H\,I}/L$, where $L \simeq 0.1$ pc, is $\langle n_{\rm H\,I}\rangle \geqslant 3.5 \times 10^3$ cm^{-3}.

The neutral hydrogen mass associated to the H I emission can be obtained assuming a spherical cloud with an H I radius of 21″ (0.1 pc) and average hydrogen density $\langle n_{\rm H\,I}\rangle \geqslant 3.5 \times 10^3$ cm^{-3}, from the expression $M({\rm H\,I}) = \frac{4\pi}{3} R^3 \langle n_{\rm H\,I}\rangle m_{\rm H\,I}$, where R is the radius of the H I emission region and $m_{\rm H\,I}$ is the hydrogen atomic mass. We obtain that the H I mass $M({\rm H\,I}) \geqslant 0.4\ M_\odot$. This value should be taken as a lower limit, since the average hydrogen density is also a lower limit. Gómez et al. (1998) used a line emission model for the PDR to estimate the total H I mass, obtaining a value as high as 5 $M_\odot$. Molecular mass estimates, derived from CO, indicate that GGD 14 has a molecular mass in the range from 640 to 1500 $M_\odot$ (Ridge et al. 2003; Higuchi et al. 2009), which means that the PDR mass is very low (<1% of the total gas mass). Of course, the PDR around G213.880−11.837 extends only over ∼1′, while the CO is detected over ∼5′ (Higuchi et al. 2009).

4.2. Kinematics of the H I Gas in GGD 14

The high optical depth toward the CH II region ($\tau_L(0) \geqslant 1$) supports the existence of high-density atomic gas, where the cometary CH II region (G213.880−11.837) is embedded. The spatial extension of the cometary H I 21 cm emission (∼42″) is ∼10 times larger than the ionized CH II region ($\leqslant 3\farcs5$ at 1.4 GHz). In the champagne model a strong density gradient is required, with the head of the cometary CH II region embedded in the densest part of the molecular clump and the ionized gas expanding asymmetrically out of the dense clump (Garay & Lizano 1999). For G213.880−11.837, Gómez et al. (1998) interpreted the kinematics of the ionized gas, derived from the H92α line, as a champagne flow due to the presence of a velocity gradient measured from the head (located to the NW with $V_{\rm LSR} \sim 11$ km s^{-1}) to the tail (located to the SE with $V_{\rm LSR} \sim 15$ km s^{-1}).

Recent numerical results show that an expanding H II region should be an efficient trigger for star formation in molecular clouds if the mass of the ambient molecular material is large enough (Hosokawa & Inutsuka 2006). In the particular case of the GGD 14 complex, a dense molecular region should exist in the vicinity of G213.880−11.837, where recently a cluster of low-mass pre-main-sequence stars has been found. In addition to the radio continuum compact sources (Gómez et al. 2000, 2002), there are infrared studies in the 2–100 μm range (Harvey et al. 1985; Hodapp 1994; Fang & Yao 2004) that provide evidence for a recently formed cluster of sources in the vicinity of G213.880−11.837. Fang & Yao (2004) estimated the age of this cluster in the order of 2–5 $\times$ 10^6 yr.

The molecular gas detected toward GGD 14 shows a complex velocity structure with the presence of a CO molecular outflow with the major axis along the NW–SE direction (P.A. $= -60^\circ$), and centered near the radio source VLA 7. In particular, we note that in the CO(2→1) images (Little et al. 1990; Qin et al. 2008), there is strong self-absorption of this line at $V_{\rm LSR} \sim 11$ km s^{-1}, which correspond to the ambient molecular gas velocity. Qin et al. (2008) show a ^{13}CO(2→1) spectrum toward this region (not affected by self-absorption) that peaks at a velocity of ∼11.5 km s^{-1}. In what follows we will assume this value for the ambient molecular gas toward GGD 14. There is also NH_3 (Torrelles et al. 1983; Güsten & Marcaide 1986; Anglada et al. 1996), CS (Anglada et al. 1996), and HCO^+ emission (Heaton et al. 1988) toward GGD 14 with velocities in the range from 9 to 12 km s^{-1}. These results point out that there is a dense region in the vicinity of the CH II region that could be responsible of the champagne morphology observed in both the CH II and the H I regions.

4.2.1. Champagne H I Flow Around G213.880−11.837?

Figure 3 shows a near-IR continuum image at 4.5 μm from the *Spitzer Space Telescope*[6] toward GGD 14. We used the processed *Spitzer* Infrared Array Camera (Fazio et al. 2004) Basic Calibrated Data (PID: 6; PI: G. Fazio), which are available in the archive of the Spitzer Science Center. In this image the stellar cluster is clearly appreciated. In this figure, we superpose a contour image of the H I 21 cm line emission (or absorption), integrated in velocity from 1 to 20 km s^{-1}. The stellar cluster is mainly located toward the H I absorption region. We note that the compact radio sources VLA 1 (G213.880−11.837) and VLA 7 have strong 4.5 μm counterparts not observed at 2.2 μm (Gómez et al. 2002), which suggests that these sources are deeply embedded. The 4.5 μm counterpart toward VLA 1 is first reported in this work, and that toward VLA 7 was recently detected by Sato et al. (2008). The near-IR source IRS 9Mc reported by Sato et al. (2008) is localized near VLA 7, and shows a bipolar infrared nebula aligned in the same direction as the bipolar molecular outflow (NW–SE; Rodríguez et al. 1982). We also note that several of the compact radio sources reported by Gómez et al. (2002), indicated with crosses, have 4.5 μm counterparts.

Figure 3 shows the velocity integrated H I 21 cm line toward G213.880−11.837, which exhibits a cometary-like morphology, resembling (at much larger scales) that of the ionized gas at high frequencies (Tofani et al. 1995; Kurtz et al. 1994; Gómez et al. 1998). The limb brightened PDR expected at the head of the cometary region G213.880−11.837 is not observed. This can be due to the H I absorption feature that

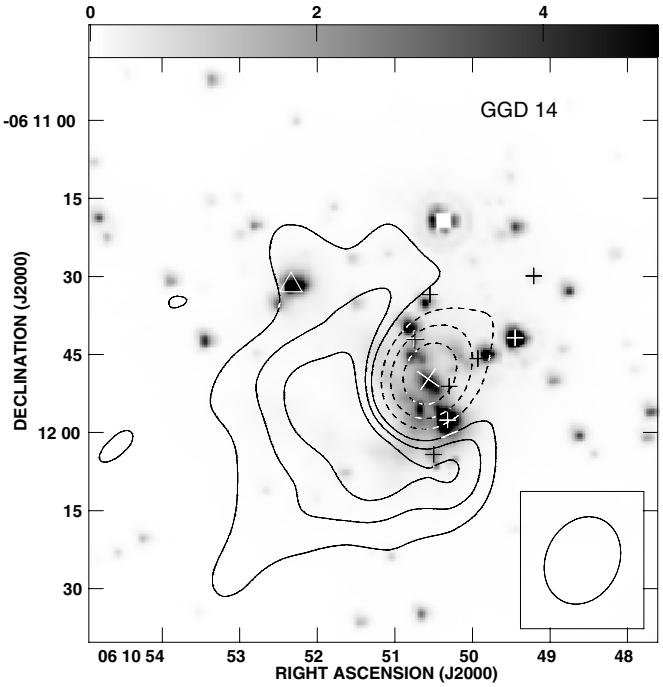

Figure 3. Superposition of the near-IR *Spitzer* image at 4.5 μm (gray scale) on the VLA integrated H I line (from 2 to 20 km s^{-1}) with solid (emission) and dashed (absorption) contours (−20, −10, −3, 3, 6, and 9 $\times$ 0.7 mJy beam^{-1} km s^{-1}). The large "×" symbol indicates the radio continuum peak position of the H II region (VLA 1) and the triangle the peak position of VLA 7. The crosses mark the peak position of the compact radio sources reported by Gómez et al. (2002).

complicates the full imaging of the PDR or to the low angular resolution of the H I observations. In the latter case, one can set a lower limit to the H I volume density at the head of the cometary. Assuming a PDR size equal to the beam size, $l = 1.5 \times 10^4$ AU $(\theta_B/15'')(d/1$ kpc), and a column density of the PDR $N_{\rm H\,I} \sim 3 \times 10^{21}$ cm^{-2} such that the dust opacity is of order unity, $n_{\rm H\,I} \geqslant N_{\rm H\,I}/l = 1.3 \times 10^4$ cm^{-3}, which is a reasonable density for molecular clouds. Molecular line observations with high spatial resolution are required to try to detect this high-density molecular gas at the head of the cometary.

In order to assess whether or not the H I emission is produced by a champagne flow, we made position–velocity diagrams of the H I emission along two perpendicular directions centered on the CH II region (peak continuum emission). The cuts are at position angles of +25° and −65° which correspond to the orientations of the minor and major axes of the ionized cometary CH II region (Gómez et al. 1998). Figure 4 shows the PV diagrams of the H I gas along these two directions. They both exhibit absorption and emission features. The spatially unresolved H I line in absorption seen at the position of the CH II region is strikingly broad in velocity, ranging from 5 to 13 km s^{-1}. We also see that at this position the H I emission reaches its maximum redshifted velocities with a value of about 18 km s^{-1}. Qin et al. (2008) have shown that the velocity of the ambient molecular gas toward GGD 14 is ∼11.5 km s^{-1}. We interpret these two features as indicating the presence of an expanding shell of H I gas around the CH II region, with an expansion velocity of about 6.5 km s^{-1}.

The PV diagram along the position of −65° shows that the emission is very extended toward the SE direction, reaching velocities in the tail of about 14 km s^{-1}. Since the ambient

[6] The *Spitzer Space Telescope* is operated by the Jet Propulsion Laboratory, California Institute of Technology under a contract with NASA.

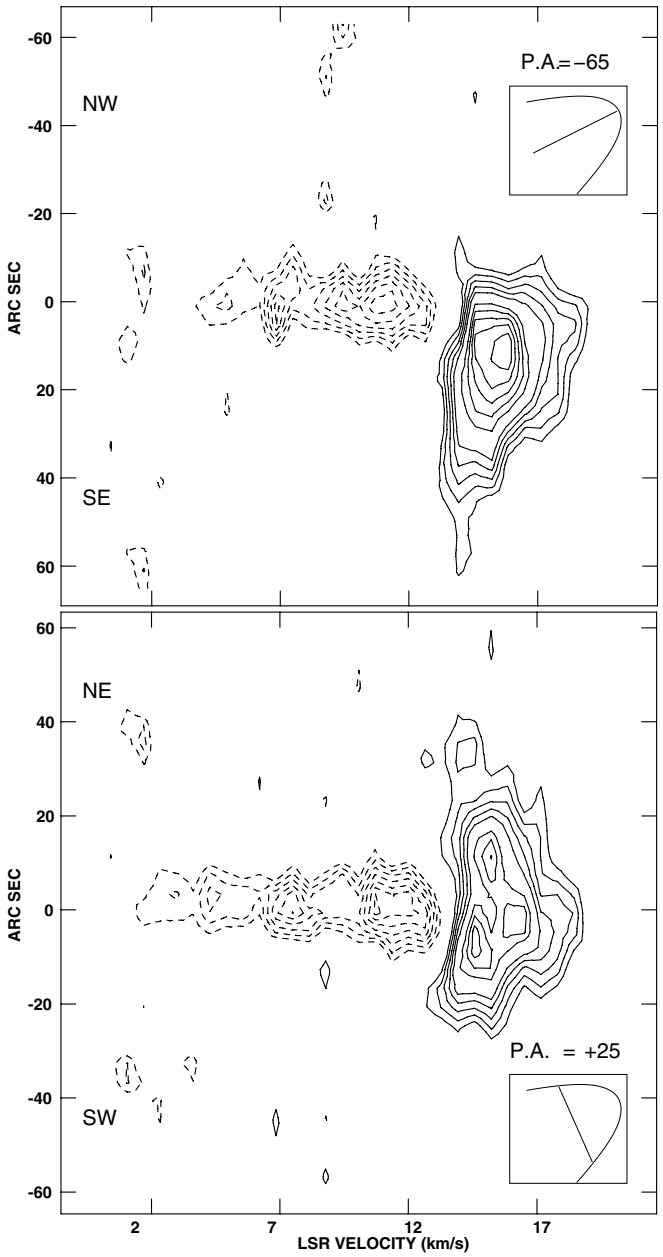

Figure 4. Position–velocity diagrams of the H I line toward GGD 14. Top: cut along the symmetry axis of the cometary H I structure (P.A. = −65°). Bottom: cut along a perpendicular direction to the symmetry axis passing through the H II region (P.A. = +25°). Contour levels are −24, −21, −18, −15, −12, −9, −6, −3, 3, 6, 9, 12, 15, and 18 × 2.5 mJy beam^{-1}, the rms noise in these images. The insets show the direction of the cuts with respect to the cometary morphology.

velocity of the molecular gas is 11.5 km s^{-1}, we interpret the PV structure seen SE of the CH II region as indicating a champagne flow of the H I gas. In a champagne flow the gas accelerates to 2–3 times the sound speed (see Table 2 of Shu et al. 2002). Since the observed velocity shift in the ionized gas is $\Delta v \sim 15$ km s^{-1} − 11 km s^{-1} = 4 km s^{-1} (Gómez et al. 1998) while a shift of $\Delta v \sim$ 20–30 km s^{-1} is expected, this ionized flow can be understood as a champagne flow only if the source is inclined close to the plane of the sky, with an angle $i < 11°$, and has a small opening angle. Gómez et al. (1998) correctly interpreted the kinematics of the ionized gas as a champagne flow but they did not estimate the inclination angle of the flow with respect to the plane of the sky, they only suggest that the tail should be going away to explain the redshifted velocities. In the present interpretation, we propose that in fact the orientation of the ionized champagne flow should be close to the plane of the sky with the tail having the redshifted velocities. On the other hand, in a PDR, one expects gas temperatures of $T \sim 500$ K, i.e., sound speeds ∼2 km s^{-1}. Thus, for a champagne flow in the H I neutral gas, the expected velocity shift is of the order of ∼4–6 km s^{-1}. Thus, the observed velocity shift, $\Delta v_{\rm H\,I} \sim 3$ km s^{-1}, is consistent with a champagne flow of the H I gas, with a large opening angle such that the observed velocity in the line of sight is small. Note that the scale of this H I flow is ∼10 times larger than the ionized champagne flow, therefore, the collimation of this H I neutral gas is probably much lower supporting the presence of a larger opening angle.

In contrast, in the cut along the perpendicular direction to the symmetry axis passing through the H II region (P.A. = +25°), the H I gas in emission is seen at both sides of the cometary head and no velocity gradient is appreciated. High angular resolution molecular observations are needed to confirm this kinematics. Another H II region that shows a cometary morphology in both the continuum and H I emission is G111.61+0.37, where a champagne interpretation was also proposed (Lebrón et al. 2001).

Hydrodynamical and radiative transfer models by Hosokawa (2007) show that an inhomogeneous medium can change the time evolution of expanding H II regions and PDRs (as compared with the evolution in a homogeneous medium). In a medium with a radial density profile of the form $n(r) \propto r^{-w}$ with $0 \leqslant w < 1$, the dense shell formed by the shock front shields the far-ultraviolet (FUV) radiation and prevents the expansion of the dissociation front beyond the shell. The CH II region is surrounded by a cold molecular envelope in this case. In a stepper density gradient with $w > 1$, as expected in a "champagne flow," shielding of the FUV radiation becomes inefficient and an extended PDR develops around the H II region. However, only if $w > 1.5$, the H_2 dissociation front propagates through the ambient cloud. Since in G213.880−11.837 and G111.61+0.37 we observe extended PDRs around the H II regions, it is likely that steep density gradients exist in both objects.

5. CONCLUSIONS

We present high angular resolution (15″) VLA observations of the H I 21 cm line toward the compact H II region G213.880−11.837. The H I gas, produced by a PDR around the CH II region, exhibits a cometary morphology with an extension, along the major axis, of ∼45″. The kinematics and morphology of the H I gas around G213.880−11.837 indicates that the neutral hydrogen gas is in expansion in a similar way as the ionized gas. In both cases, the gas accelerates toward lower density regions and redshifted velocities (from ∼11 to 14 km s^{-1}). The peak position of the H I absorption coincides with the peak continuum emission of the CH II region (VLA 1; G213.880−11.837). This is the second (after G111.61+0.37) cometary H II/H I region known. These observations suggest the existence of champagne flows in PDRs associated with cometary H II regions.

We thank an anonymous referee for the comments and suggestions that helped to improve this paper. Y.G., L.F.R., and S.L. acknowledge support from DGAPA-UNAM and CONACyT

Mexico. G.G. acknowledges support from CONICYT projects FONDAP 15010003 and BASAL PFB-06.

REFERENCES

Anglada, G., Estalella, R., Pastor, J., Rodríguez, L. F., & Haschick, A. D. 1996, ApJ, 463, 205
Briggs, D. 1995, PhD thesis, New Mexico Institute of Mining and Technology
Brogan, C. L., Troland, T. H., Roberts, D. A., & Crutcher, R. M. 1999, ApJ, 515, 304
Cappa, C., Niemela, V. S., Amorín, R., & Vasquez, J. 2008, A&A, 477, 173
Eisloffel, J., Mundt, R., Ray, T. P., & Rodríguez, L. F. 2000, Protostars and Planets IV (Tucson, AZ: Univ. Arizona Press), 815
Fang, M., & Yao, Y. Q. 2004, ChA&A, 28, 308
Fazio, G. G., et al. 2004, ApJS, 154, 10
Garay, G., Gómez, Y., Lizano, S., & Brown, R. L. 1998, ApJ, 501, 699
Garay, G., & Lizano, S. 1999, PASP, 111, 1049
Gómez, Y., Lebrón, M., Rodríguez, L. F., Garay, G., Lizano, S., Escalante, V., & Cantó, J. 1998, ApJ, 503, 297
Gómez, Y., Rodríguez, L. F., & Garay, G. 2000, ApJ, 531, 861
Gómez, Y., Rodríguez, L. F., & Garay, G. 2002, ApJ, 571, 901
Güsten, R., & Marcaide, J. M. 1986, A&A, 164, 342
Gyulbudaghian, A. L., Glushkov, Yu. I., & Denisyuk, E. K. 1978, ApJ, 224, L137
Harvey, P. M., Wilking, B. A., Joy, M., & Lester, D. F. 1985, ApJ, 288, 725
Heaton, B. D., Little, L. T., Andersson, M., & Dent, W. R. F. 1988, A&A, 203, 99
Higuchi, A. E., Yasutaka, K., Masao, S., & Ryohei, K. 2009, ApJ, 705, 468
Hodapp, K. W. 1994, ApJS, 94, 615
Hollenbach, D. J., & Tielens, A. G. G. M. 1997, ARA&A, 35, 179
Hosokawa, T. 2007, A&A, 463, 187
Hosokawa, T., & Inutsuka, S.-i. 2006, ApJ, 646, 240
Kurtz, S., Churchwell, E., & Wood, D. O. S. 1994, ApJS, 91, 659
Lebrón, M., & Rodríguez, L. F. 1997, RevMexAA, 33, 165
Lebrón, M. E., Rodríguez, L. F., & Lizano, S. 2001, ApJ, 560, 806
Little, L. T., Heaton, B. D., & Dent, W. R. F. 1990, A&A, 232, 173
Qin, S.-L., Wang, J.-J., Zhao, G., Miller, M., & Zhao, J.-H. 2008, A&A, 484, 361
Ridge, N. A., Wilson, T. L., Megeath, S. T., Allen, L. E., & Myers, P. C. 2003, AJ, 126, 286
Rodríguez, L. F., Carral, P., Ho, P. T. P., & Moran, J. M. 1982, ApJ, 260, 635
Rodríguez, L. F., Moran, J. M., Ho, P. T. P., & Gottlieb, W. 1980, ApJ, 235, 845
Rohlfs, K., & Wilson, T. L. 2003, Tools of Radio Astronomy (4th ed.; Berlin: Springer), 319
Sato, Y., et al. 2008, PASJ, 60, S429
Shu, F. H., Lizano, S., Galli, D., Cantó, J., & Laughlin, G. 2002, ApJ, 580, 969
Tofani, G., Felli, M., Taylor, G. B., & Hunter, T. R. 1995, A&AS, 112, 299
Torrelles, J. M., Rodríguez, L. F., Cantó, J., Carral, P., Marcaide, J., Moran, J. M., & Ho, P. T. P. 1983, ApJ, 274, 214
Torrelles, J. M., Verdes-Montenegro, L., Ho, P. T. P., Rodríguez, L. F., & Cantó, J. 1989, ApJ, 346, 756